

# Photoproducts of Bacteriorhodopsin Mutants: A Molecular Dynamics Study

William Humphrey,\* Ernst Bamberg,# and Klaus Schulten\*

\*Beckman Institute and Department of Physics, University of Illinois at Urbana-Champaign, Urbana, Illinois 61801 USA, and #Department of Biophysical Chemistry, Max-Planck-Institut für Biophysik, D-60596 Frankfurt, Germany

**ABSTRACT** Molecular dynamics simulations of wild-type bacteriorhodopsin (bR) and of its D85N, D85T, D212N, and Y57F mutants have been carried out to investigate possible differences in the photoproducts of these proteins. For each mutant, a series of 50 molecular dynamics simulations of the photoisomerization and subsequent relaxation process were completed. The photoproducts can be classified into four distinct classes: 1) 13-*cis* retinal, with the retinal N-H<sup>+</sup> bond oriented toward Asp-96; 2) 13-*cis* retinal, with the N-H<sup>+</sup> oriented toward Asp-85 and hydrogen-bonded to a water molecule; 3) 13,14-*di-cis* retinal; 4) *all-trans* retinal. Simulations of wild-type bR and of its Y57F mutant resulted mainly in class 1 and class 2 products; simulations of D85N, D85T, and D212N mutants resulted almost entirely in class 1 products. The results support the suggestion that only class 2 products initiate a functional pump cycle. The formation of class 1 products for the D85N, D85T, and D212N mutants can explain the reversal of proton pumping under illumination by blue and yellow light.

## INTRODUCTION

To maintain a proton gradient across the bacterial cell membrane, *Halobacterium salinarium* under anaerobic conditions will express the protein bacteriorhodopsin (bR), which functions as a light-driven proton pump (Oesterhelt and Stoekenius, 1973). The pump derives energy through absorption of a photon by a retinal chromophore, bound via a protonated Schiff base linkage to a lysine residue. Recent reviews discuss the structure and proton pump function of bR (Oesterhelt et al., 1992; Ebrey, 1993; Schulten et al., 1995).

It is generally accepted that the bR proton pump cycle starts in the so-called bR<sub>568</sub> state, in which the protein contains *all-trans* retinal and absorbs at 568 nm. Light absorption induces photoisomerization of retinal about its C<sub>13</sub>-C<sub>14</sub> bond to form within 5 ps a first intermediate, referred to as K<sub>590</sub>, the subscript indicating the absorption maximum in nanometers. The K<sub>590</sub> intermediate relaxes, within 40 μs, to an intermediate referred to as L<sub>550</sub> (Lozier et al., 1975), at which stage the retinal Schiff base proton is transferred to the residue Asp-85 and bR forms the so-called M<sub>412</sub> intermediate, which exhibits a strong blue shift due to the deprotonation of the retinal Schiff base. On a millisecond time scale, the retinal Schiff base becomes reprotonated and forms the intermediate N<sub>520</sub>, the proton being donated from the residue Asp-96, located near the cytoplasmic side of the membrane. In the N<sub>520</sub> state, retinal thermally re-isomerizes to the *all-trans* form, resulting in the so-called

O<sub>640</sub> intermediate; the latter decays to the initial bR<sub>568</sub> state (Lanyi, 1992).

FTIR spectroscopy and observations of bR mutants have identified residues directly involved in the proton pump pathway, namely Asp-85 (Mogi et al., 1988; Subramaniam et al., 1990; Otto et al., 1990), Asp-212 (Mogi et al., 1988; Otto et al., 1990), Asp-96 (Mogi et al., 1988; Holz et al., 1989), and Glu-204 (Brown et al., 1995; Balashov et al., 1995; Richter et al., 1996). These findings have been corroborated by the three-dimensional structure of bR<sub>568</sub>, determined by electron cryomicroscopy (Henderson et al., 1990), which revealed a channel involving the mentioned residues. Early observations of dehydration effects (Korenstein and Hess, 1977) as well as neutron diffraction studies (Papadopoulos et al., 1990), FTIR spectra (Maeda et al., 1994), and molecular dynamics simulations (Zhou et al., 1993; Humphrey et al., 1994, 1995) also attribute to water molecules an active role in the proton pump activity of bR. Fig. 1 provides a view of bR<sub>568</sub> that exhibits water molecules in the proton channel as well as key residues. Several water molecules are seen in Fig. 1 to form a network of hydrogen bonds with charged and polar amino acids near the Schiff base linkage of retinal; three water molecules (W<sub>A</sub>, W<sub>B</sub>, W<sub>C</sub>) interact directly with the Schiff base N-H<sup>+</sup>, water W<sub>A</sub> being directly hydrogen-bonded to the Schiff base in bR<sub>568</sub>.

Even though the proton channel has been structurally identified, it is still an open question how protons are transferred irreversibly between the cytoplasmic and the extracellular side of bR. MD simulations of the picosecond (Humphrey et al., 1995; Xu et al., 1996), nanosecond to microsecond (Humphrey et al., 1995), and later (Xu et al., 1995) intermediates of the pump cycle suggest that the irreversible transfer of protons requires the photoisomerization of retinal toward a torsionally deformed 13-*cis* geometry that is stabilized through a strong interaction of the Schiff base proton with a water molecule forming a bridge

Received for publication 12 August 1996 and in final form 22 November 1996.

Address reprint requests to Dr. Klaus Schulten, Department of Physics, Beckman Institute 3147, University of Illinois, 405 N. Mathews Ave., Urbana, IL 61801. Tel.: 217-244-2212; Fax: 217-244-6078; E-mail: kschulte@ks.uiuc.edu.

© 1997 by the Biophysical Society

0006-3495/97/03/1347/10 \$2.00

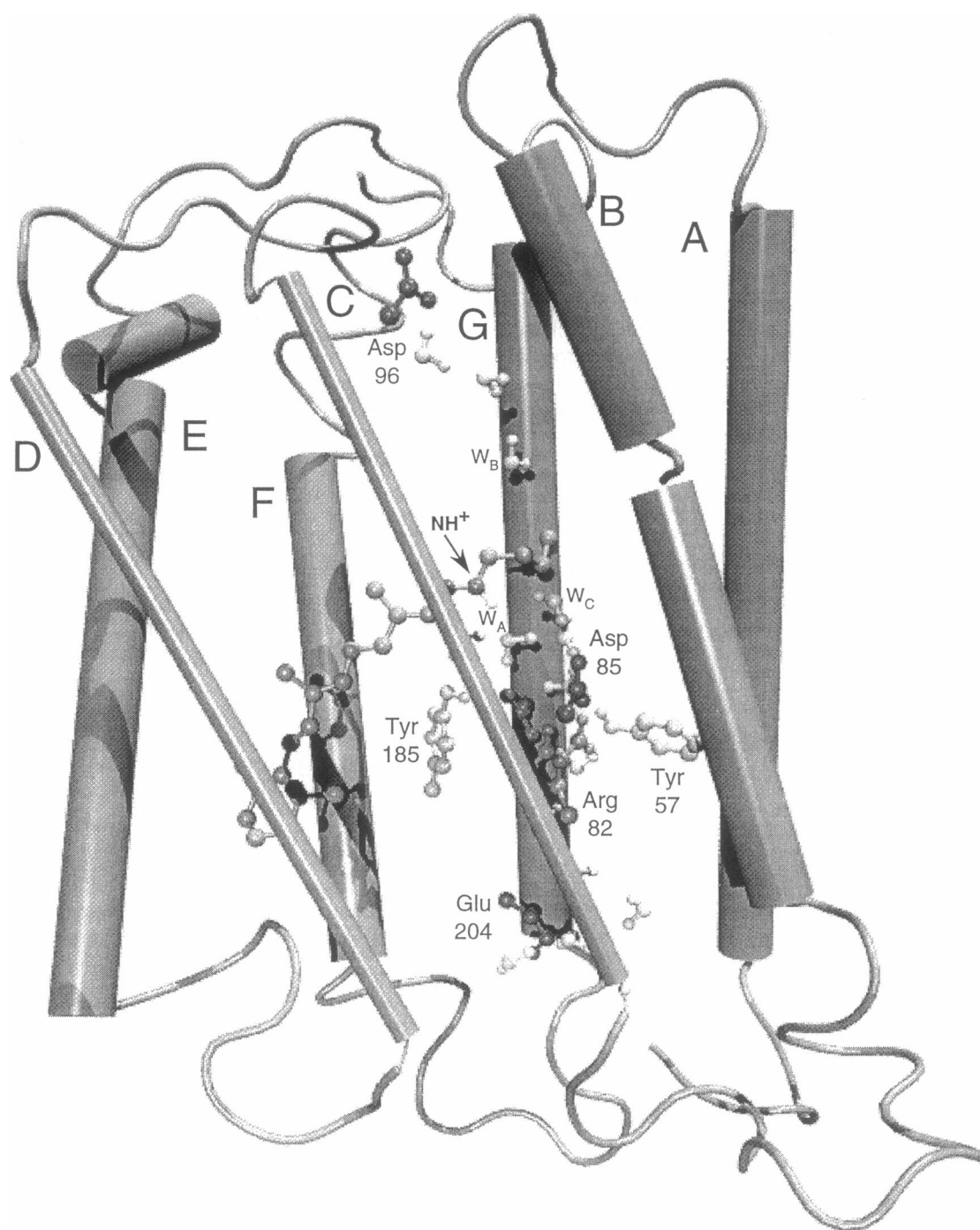


**FIGURE 1** Refined bacteriorhodopsin bR<sub>568</sub> structure (Humphrey et al., 1994) used as a starting point in the simulations reported. Shown are the seven transmembrane helices of bR along with internal water molecules and key residues participating in the proton pump cycle. Helices C and D are presented as thin cylinders to reveal the protein interior.

to Asp-85. If such a photoproduct is not formed, bR does not pump protons in the desired outward direction. Resolution of the crucial retinal geometry presently defies available experimental methods. In this article we resort to the study of various bR mutants by means of MD simulations to investigate the extent to which the occurrence of the stated retinal photoproduct relates to the pump behavior observed for the mutants.

Site-directed mutagenesis experiments have already contributed much to our understanding of the function of bR. Experiments involving bR mutants D85{N,T,E,A} (Mogi et al., 1988; Subramaniam et al., 1990; Otto et al., 1990) have pointed to the role of the negatively charged Asp-85 as the initial acceptor of retinal's Schiff base proton, whereas studies of mutants D212{N,E,A} (Mogi et al., 1988; Otto et al., 1990) and R82{A,Q,K} (Subramaniam et al., 1990; Otto

et al., 1990; Balashov et al., 1995) have shown these ionic groups near retinal to control the yield of the pump. Site-directed mutagenesis has also pointed to Glu-204 as the group responsible for accepting the proton from Asp-85, before releasing it to the extracellular domain (Brown et al., 1995; Balashov et al., 1995; Richter et al., 1996).

Mutants of bR in which residue Asp-85 or Asp-212 is replaced by neutral or positively charged groups, such as asparagine or threonine, exhibit dramatic differences in their proton pump behavior and, accordingly, were chosen as the subject of our investigation. At physiological pH, photoisomerization to early intermediates with close similarities to K<sub>590</sub> and L<sub>550</sub> of native bR arise, but proton pumping is abolished and an intermediate with a deprotonated retinal Schiff base is not formed (Mogi et al., 1988; Needleman et al., 1991). Mutation of Asp-85 in bR to a nonnegative residue results in a significant change in the pK<sub>a</sub> of the Schiff base, lowering it in many cases by 5–7 units (Otto et al., 1990). Replacement of Asp-85 by asparagine or threonine can result in a reversal of the direction of proton transfer, when yellow and blue light is applied and two photons are absorbed in a cycle (Tittor et al., 1994, 1995). The resulting pump action is similar to that of the homologous chloride-pumping protein halorhodopsin (hR), which contains a threonine residue at the position corresponding to Asp-85 in bR; employing two photons, hR can also pump protons inwardly (Bamberg et al., 1992).

In this paper we compare the photoisomerization products, as described by means of MD simulations, of wild-type bR and of bR's D85N, D85T, D212N, and Y57F mutants. The current study is a follow-up of our previous MD simulations of the wild-type early intermediates (Humphrey et al., 1995), employing the same simulation and analysis methods to investigate the photoreaction of bR mutants as well as the wild type. In Materials and Methods we describe the construction of the bR mutants studied and simulation of the photoisomerization reaction. In Results the outcomes of the photoproducts are presented. In the Discussion we compare these results to earlier simulations of the wild-type photocycle and derive a model that can explain how the D85N and D85T mutants of bR can pump protons in the direction opposite that of wild-type bR.

## MATERIALS AND METHODS

Molecular dynamics calculations described in this report were performed using the programs NAMD (Nelson et al., 1996) and X-PLOR (Brünger, 1988), both of which implement the CHARMM force field (Brooks et al., 1983). The simulations were carried out in vacuum at a temperature of 300 K, using a dielectric constant of  $\epsilon = 1$  and a 12-Å cutoff of Coulomb forces. All calculations used the CHARMM-19 parameters and topology for the modeling of bR, with the exception of retinal. Simulations were carried out both with and without an explicit hydrogen-bond term in the force field. The CHARMM-19 parameters were preferred over more recent releases to allow comparison with previous simulations of native bR. Simulations employing CHARMM-22 parameters did not exhibit major differences from simulations using CHARMM-19 parameters.

The previously reported structure of bR<sub>568</sub> (Fig. 1), refined by means of molecular dynamics simulations (Humphrey et al., 1994), was used as a

starting point for all simulations of bR<sub>568</sub>, and served as the initial structure for the modeling of bR mutants. After initial construction, each mutant structure underwent 1000 steps of energy minimization, followed by a 15-ps MD simulation with frequent velocity rescaling to heat the system to 300 K, and a 5-ps MD simulation at 300 K with infrequent velocity rescaling. Harmonic restraints were applied to the oxygen atoms of the water molecules during this equilibration to maintain their positions.

The retinal charges, parameters, and modeling procedures for the photoisomerization process employed here were the same as those employed in the previous study (Humphrey et al., 1995). The photoisomerization procedure had been explained earlier as well in terms of ground- and excited-state potential energy surfaces evaluated quantum chemically (Schulten et al., 1995). Accordingly, retinal was induced to rotate about the C<sub>13</sub>-C<sub>14</sub> bond using the following procedure:

1. At  $t = 0$ , the conventional ground-state energy surface governing torsion around the C<sub>13</sub>-C<sub>14</sub> bond was replaced by a potential surface describing the excited state with maxima at the all-*trans* and the 13-*cis* positions and a minimum at 90°.
2. At  $t = 250$  fs, this potential surface was switched to one describing intersystem crossing and exhibiting a maximum at the all-*trans* position and a single minimum at 13-*cis*.
3. At  $t = 500$  fs, the conventional ground-state energy surface with minima at the all-*trans* and the 13-*cis* positions was reinstalled for a period of 2.5 ps.

All simulations were carried out at  $T = 300$  K. In all cases a barrier of 10 kcal/mol inhibited torsion around the C<sub>14</sub>-C<sub>15</sub> single bond.

After the construction and equilibration of the initial (all-*trans*) structure for each mutant, the systems were simulated for an additional 20 ps and the root mean square difference (RMSD) of each C <sub>$\alpha$</sub>  atom was determined. The resulting RMSD for wild-type bR and its D85N, D85T, D212N, and Y57F mutants exhibited average values ranging between 0.5 Å and 2 Å, reflecting the structural stability of the bR mutants. Similar results were obtained for the RMSDs of the positions of water molecules.

MD simulations were then performed to model the initial photoisomerization reaction of bR<sub>568</sub>. As in the previous study (Humphrey et al., 1995), 50 independent simulations were performed, starting from the same protein configuration, but with different velocities chosen randomly from a Maxwell distribution at 300 K. After the initial velocity assignment, 100 fs of dynamics were performed, after which the simulated 3-ps photoisomerization reaction was carried out as described above. The overall procedure, summarized in Fig. 2, resulted in a set of 50 photoproducts for each mutant.

## RESULTS

The photoproducts resulting from each set of 50 simulated photoisomerization reactions for wild-type bR and its D85N, D85T, D212N, and Y57F mutants have been categorized based on the final configuration of the water molecules and the orientation of the N-H<sup>+</sup> bond. To measure the latter orientation we determined the angle  $\theta_{SB}$  between the line through the N-H<sup>+</sup> group of retinal and the line connecting the Schiff base nitrogen with the carboxyl of Asp-96 (see Fig. 1). Four distinct sets of photoproducts,

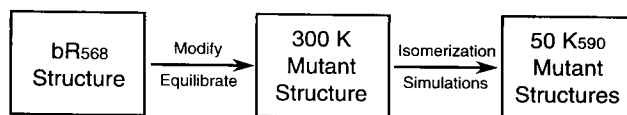


FIGURE 2 Schematic representation of the protocol used to construct and simulate the photoisomerization of bacteriorhodopsin mutants. The isomerization simulations followed the same schedule as used by Humphrey et al. (1995).

referred to below as case 1–4 products, were identified through the value of  $\theta_{SB}$ : case 1 photoproducts contained a 13-*cis* retinal with a  $\theta_{SB}$  of less than  $60^\circ$ , indicating a Schiff base proton oriented toward Asp-96; case 2 photoproducts also contained a 13-*cis* retinal, but with a  $\theta_{SB}$  value near  $90^\circ$ , indicating a twisted retinal with an N-H<sup>+</sup> bond oriented toward Asp-85; case 3 photoproducts contained 13,14-*di-cis* retinal; case 4 photoproducts resulted when the isomerization failed to complete and retinal remained all-*trans*. The case 1 trials often contained a hydrogen bond between the Schiff base and water  $W_B$ ; all case 2 trials had a hydrogen bond between water  $W_C$  and retinal.

Table 1 summarizes the results of the simulated photoisomerizations. In all mutants studied, case 1 and case 2 photoproducts (those containing a 13-*cis* retinal) accounted for at least 78% of all photoproducts, and only these cases are included in the table. The table entries state the observed fractions of case 1 and case 2 photoproducts, as well as what percentage of the case 1 or case 2 photoproducts resulted from a clockwise isomerization, the rotation direction being defined by looking from the Schiff base nitrogen toward retinal's  $\beta$ -ionone ring. A clockwise isomerization corresponds to a motion in which the Schiff base N-H<sup>+</sup> bond passes closer to the Asp-85 residue rather than the Asp-212 residue.  $E_{SB}$  given in Table 1 is the electrostatic interaction energy between the Schiff base proton and the surrounding protein environment, averaged over all photoproducts corresponding to a specific case.  $\Delta E_{SB}$  measures the difference of the same electrostatic energy between the final photoproduct and the initial state (i.e., with all-*trans* retinal).

The simulations of the bR photoisomerization reaction were carried out in two ways, the first including an explicit hydrogen-bond term in the molecular dynamics energy function, the second omitting this term. The values in Table 1 include the yield of case 1 and case 2 photoproducts for both sets of simulations, but provide the rotational motion and retinal energy data only for the simulations involving an explicit hydrogen-bond term. Inclusion of the hydrogen-bond term primarily affected the relative yield of case 1 and case 2 photoproducts for the bR wild-type and Y57F mutants; the remaining values reported in Table 1 were quite similar in the two series of molecular dynamics calculations.

## bR<sub>568</sub>

As a point of reference we consider first the results of simulated photoisomerizations for wild-type bR. We have extended previous simulations (Humphrey et al., 1995) to confirm the earlier findings and to ensure proper comparison with the simulations of bR mutants discussed further below. In this study, 62% of the trials resulted in case 1 structures, and 32% of the trials resulted in case 2 structures; the remaining 6% of the cases failed to isomerize and remained all-*trans*. In the previous simulations (Humphrey et al., 1995), case 1 and case 2 photoproducts for the wild type occurred with similar frequency (58% and 36%, respectively). Case 2 structures arise through hydrogen bonding with water  $W_C$  as shown in Fig. 3 *b*, which helps stabilize the twisted retinal geometry; this is highlighted by the reduction of the case 2 photoproduct yield in simulations without an explicit hydrogen-bond energy term. In the latter case, 66% of the trials form case 1 structures, and only 20% form case 2 photoproducts.

Although case 1 structures occurred more frequently than case 2 structures, it was argued in the previous report (Humphrey et al., 1995) that case 2 photoproducts actually represent the K<sub>590</sub> intermediate, which initiates a pumping cycle; case 1 structures lack a pathway for transfer of the Schiff base proton to Asp-85 and either do not arise upon excitation of bR<sub>568</sub>, or they initiate a separate nonpumping (idle) sequence, characterized through the lack of a deprotonated retinal Schiff base intermediate in the cycle. Although the simulated photoisomerizations may not capture quantitatively the propensity of the various photoproducts, they have identified a viable candidate for the K<sub>590</sub> structure and may, furthermore, properly describe how mutations affect the quantum yield of various photoproducts. In this respect it is important to note that combined classical/quantum mechanical simulations of the photoisomerization carried out recently (in preparation) and based on quantum chemically evaluated potential surfaces (Schulten et al., 1995) yield analogous isomerization products with a significantly higher yield of case 2 products. Furthermore, the recent simulations result in more all-*trans* products, in accordance with the quantum yield of the photoreaction.

**TABLE 1** Summary of simulation results for case 1, 2 photoproducts (see text)

	Case 1					Case 2				
	bR <sub>568</sub>	D85N	D85T	D212N	Y57F	bR <sub>568</sub>	D85N	D85T	D212N	Y57F
w/HB frequency*	0.62	0.78	0.84	0.98	0.44	0.32	0.00	0.00	0.02	0.38
wo/HB frequency*	0.66	0.86	0.94	0.98	0.52	0.20	0.02	0.06	0.00	0.32
CW rotation*	0.00	0.38	0.67	0.04	0.00	0.00	—	—	1.00	0.16
$E_{SB}$ (kcal/mol)*	-19.3	-6.5	-8.9	-7.7	-18.4	-32.2	—	—	-22.3	-31.3
$\Delta E_{SB}$ (kcal/mol)*	15.0	14.3	15.0	14.6	15.3	2.2	—	—	-0.4	2.2

\*Results for simulations including an explicit hydrogen-bond interaction term.

#Results for simulations without an explicit hydrogen-bond interaction term.

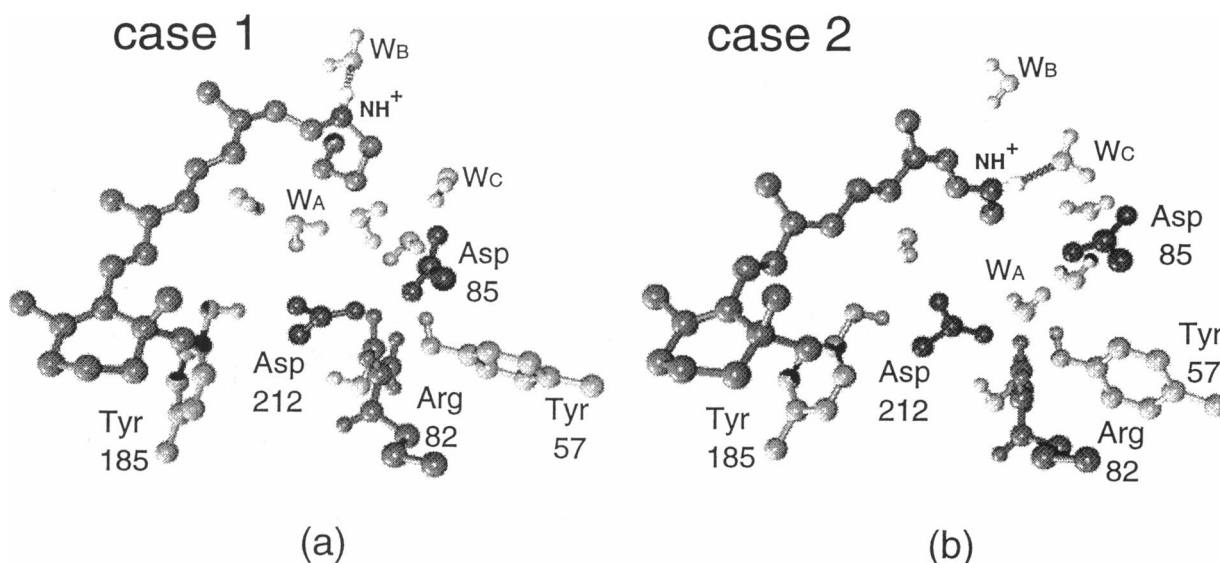


FIGURE 3 Structure of the retinal binding site of the case 1 and case 2 photoproducts of wild-type bacteriorhodopsin, including water molecules and key residues participating in the proton pump cycle. (a) Sample case 1 product, with the Schiff base proton connected to the cytoplasmic channel and hydrogen bonded to water  $W_B$ . (b) Sample case 2 product, exhibiting a Schiff base proton connected to the extracellular channel via a hydrogen bond with water  $W_C$ .

Figure 3 presents two structures corresponding to case 1 and case 2 photoproducts of  $bR_{568}$ . One can recognize that in case 2 the Schiff base proton is favorably positioned to be transferred via  $W_C$  to Asp-85, whereas in case 1 the proton is pointing toward Asp-96, i.e., in the wrong direction. Energetic analysis reveals that for case 2 photoproducts retinal assumes a twisted (i.e., energetically unfavorable) geometry that is stabilized through a strong hydrogen bond with water  $W_C$ .

The electrostatic interaction energy of the Schiff base proton ( $E_{SB}$ ) for case 2 photoproducts lies 12.9 kcal/mol below that of case 1 photoproducts;  $\Delta E_{SB}$ , for case 2 photoproducts, is close to zero (2.2 kcal/mol), whereas for case 1 photoproducts the Schiff base proton electrostatic energy increases by 15.0 kcal/mol. This difference arises from the Schiff base, in case 2, being closer to the negatively charged aspartic acids and to polar water molecules than in case 1 and forming a stronger hydrogen bond with water.

### D85N and D85T mutants

Modification of the negatively charged Asp-85, the primary proton acceptor in the wild-type photocycle, to a neutral residue such as arginine or threonine has been shown to cause a 5- to 6-unit drop in retinal's Schiff base  $pK_a$  (Mogi et al., 1988; Subramaniam et al., 1990). Simulations of Asp-85 mutants described here were performed using a protonated Schiff base; thus they relate to experiments done at sufficiently low pH to maintain the Schiff base in a protonated state.

Simulated photoisomerization of the D85N mutant resulted in a large number of case 1 photoproducts (78%), an

example of which is shown in Fig. 4 *a*. For this mutant, no case 2 structures arose, with the remaining 22% of photoisomerization processes resulting in either 13,14-*di-cis* (case 3) or all-*trans* (case 4) retinal. When simulated without an explicit hydrogen-bond term, the D85N mutant exhibited an equally large frequency of case 1 photoproducts (86%), and an equally small yield of case 2 structures. The direction of rotation was primarily counterclockwise, as for case 1 photoproducts of wild-type  $bR_{568}$ . Because of the loss of a negative charge on residue 85,  $E_{SB}$  is significantly more positive for the D85N case 1 photoproducts as compared to the value for wild-type case 1 photoproducts. However, the change in  $E_{SB}$  for case 1 D85N products, 14.3 kcal/mol, is very close to the corresponding value for  $bR_{568}$  case 1 products.

Simulated photoisomerization of the D85T mutant resulted in a distribution of photoproducts similar to that of the D85N mutant, with the difference being a slightly (6%) higher fraction of case 1 photoproducts. The same is true for the simulations without hydrogen-bond interactions, except for a slight (6%) yield of case 2 D85T structures not seen in the calculations with a hydrogen-bond term. In D85T case 1 simulations,  $E_{SB}$  is more positive than the value of  $E_{SB}$  for  $bR_{568}$  case 1 photoproducts, which is due, in the same way as seen for D85N, to the loss of a negative charge on residue 85. Also for case 1 photoproducts in the D85T simulations, the value for  $\Delta E_{SB}$  is close to that for  $bR_{568}$ ; this result is comparable to the situation for D85N as well. The major differences between the D85T and D85N simulations are a preferred clockwise rotation direction in all D85T isomerization simulations, and a lower value for  $E_{SB}$ . Fig. 4 *b* shows a case 1 photoproduct of the D85T mutant.

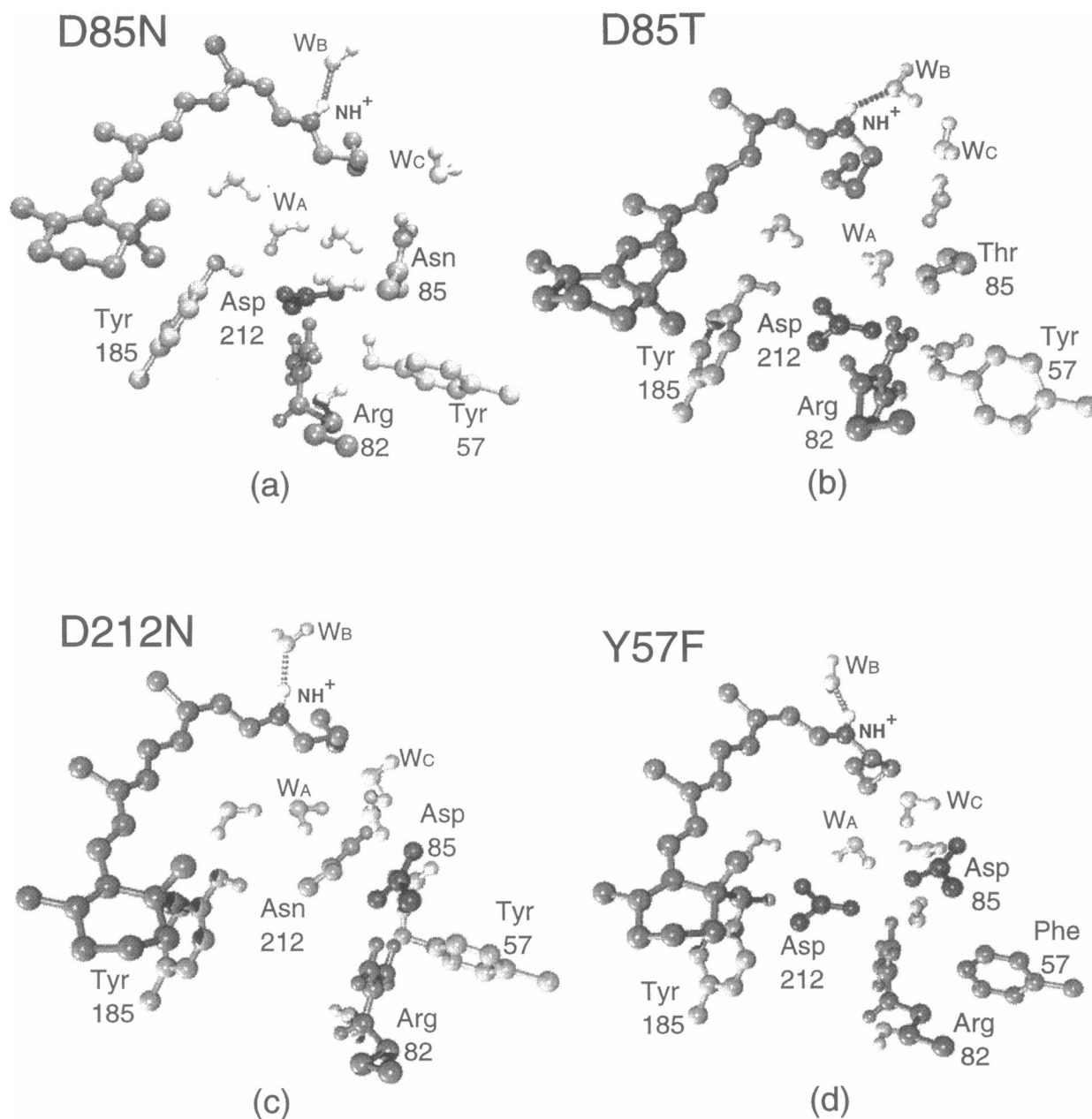


FIGURE 4 Structure of the retinal binding site of the case 1 photoproducts of several bR mutants. (a) D85N; (b) D85T; (c) D212N; (d) Y57F.

### D212N mutant

Simulations of the D212N mutant of bR were carried out assuming a protonated Schiff base. This is reasonable, as mutation of Asp-212 to a neutral form does not significantly lower the Schiff base  $pK_a$  (Subramaniam et al., 1990). The D212N mutant is of interest because at neutral pH light absorption by the mutant leads neither to a deprotonated retinal Schiff base intermediate nor to an active pump cycle (Mogi et al., 1988). Simulated photoisomerization for this mutant resulted always in case 1 photoproducts, with the exception of a single case 2 occurrence. No case 2 photo-

products arose in any of the D212N simulations that did not include a hydrogen-bond term. As in wild-type and D85N photoisomerizations, but contrary to the behavior for the D85T mutant, case 1 photoproducts arose from counter-clockwise rotation. Fig. 4 *c* shows a case 1 photoproduct of the D212N mutant. Because of the loss of a negative charge in the counterion region as a result of the D212N mutation, the electrostatic energy of the Schiff base proton for case 1 photoproducts is comparable to that for the same photoproducts of the D85N and D85T mutants.  $\Delta E_{SB}$  is also close to the values for both the D85N and D85T mutants for the case 1 photoproducts.

## Y57F mutant

Of the mutations considered in this study, the Y57F mutation produces the smallest perturbation to the retinal binding site, a loss of two hydrogen-bond participants due to the removal of the tyrosine hydroxyl. Indeed, light absorption by Y57F mutants induces an unprotonated retinal Schiff base intermediate as well as proton pumping (Govindjee et al., 1995). Simulated photoisomerization yielded a distribution containing 44% case 1 and 38% case 2 photoproducts; of the remaining nine trials, seven failed to complete the isomerization and remained in an all-*trans* state, and the remaining two trials produced a 13,14-di-*cis* retinal. A similar distribution of trials was seen when simulated without an explicit hydrogen-bond term. This distribution is closer to that seen for the wild type than for any of the other mutants considered here. With regard to the rotation direction and the Schiff base proton interaction energy, Y57F acts much like the wild-type. A case 1 photoproduct of the Y57F mutant is shown in Fig. 4 *d*.

## DISCUSSION

In the simulations of bR and its mutants, the photoreactions completed with few exceptions the isomerization around the C<sub>13</sub>-C<sub>14</sub> bond of retinal within 500 fs. The vast majority of the trials formed case 1 and case 2 photoproducts (see Figs. 3 and 4), in proportions that depended on the particular mutant studied. As pointed out above, earlier studies (Humphrey et al., 1995; Schulten et al., 1995) suggested that case 2 photoproducts represent the structure of the K<sub>590</sub> intermediate that actually initiates the proton pump cycle. In the previous study, two model potentials governing the excited-state isomerization dynamics were considered: a surface with a 10 kcal/mol barrier against torsion of the C<sub>14</sub>-C<sub>15</sub> bond and a surface in which this barrier had been reduced to 2 kcal/mol (Humphrey et al., 1995). The simulations reported here employed only the first potential, which has a larger propensity to form case 1 and case 2 photoproducts rather than case 3 photoproducts.

### Lack of case 2 products for D85N, D85T, and D212N bR

For wild-type bR, 32% of the simulated photoproducts form case 2 structures. The Y57F mutant, which has been shown to undergo a functional photocycle with a deprotonated retinal Schiff base intermediate (Govindjee et al., 1995), forms case 2 photoproducts in 38% of the simulated isomerization reactions. The D85N, D85T, and D212N mutants, in contrast to the functional wild-type and Y57F mutants, represent nonfunctional systems, and do not form case 2 structures to any significant degree. In fact, replacement of Asp-85 by neutral residues has been observed to eliminate proton pumping activity (Mogi et al., 1988; Subramaniam et al., 1990; Otto et al., 1990), and D212N mutants engage in photocycles without a deprotonated retinal Schiff base (for

pH values above 7) and form only a small fraction of deprotonated intermediates at lower pH values (Needleman et al., 1991). Thus the occurrence of case 2 photoproducts in the mutants studied correlates with the proton pumping activity of these mutants. This supports the suggestion that case 2 structures represent the functionally important K<sub>590</sub> intermediate (Humphrey et al., 1995; Schulten et al., 1995).

### Energetics of case 1 and case 2 photoproducts

How is the formation of case 1 and case 2 photoproducts controlled by native bR and its mutants? The lack of the primary proton acceptor group in the D85N and D85T mutants could be considered the primary reason for the lack of M<sub>412</sub> formation in these mutants. However, D212N, which also fails to form a deprotonated retinal intermediate, does contain the proton acceptor Asp-85, which suggests that the reason for the elimination of pumping activity in certain bR mutants is due to electrostatic interactions.  $\Delta E_{SB}$ , which measures the net electrostatic interaction between the Schiff base proton and the surrounding protein, differs significantly between case 1 and case 2 photoproducts for each mutant. The values of  $\Delta E_{SB}$  for case 1 products are all in the range 13–16 kcal/mol, for both functional and nonfunctional mutants, whereas for case 2 products the values of  $\Delta E_{SB}$  are close to zero. The hydrogen bond of the Schiff base proton to water W<sub>C</sub> (see Fig. 3 *b*) stabilizes case 2 structures and maintains a pathway for proton transfer to Asp-85, and the loss of electrostatic attraction when a neutral residue replaces Asp-85 or Asp-212 destabilizes case 2 structures. This can explain why mutation of Asp-212 eliminates pumping activity, even though the Asp-85 proton acceptor is available: both mutations destabilize case 2 photoproducts and disrupt the retinal hydrogen-bond connection to the counterion vicinity.

### Need to improve the description of the photoproduct yields

A serious shortcoming of the present description is the low yield of case 2 photoproducts, which are suggested to initiate bR<sub>568</sub>'s pump cycle, relative to case 1 photoproducts. The yield depends sensitively on the depth and on the range of the potential energy well corresponding to the formation of hydrogen bonds to water W<sub>C</sub>. Accurate calculations of potential energy surfaces within an error margin required to predict accurate yields are beyond the scope of the force field model used in our simulation; quantitative predictions of the quantum yields of bR<sub>568</sub>'s photoisomerization require essential improvements of the force field used, at least of the force field governing the photodynamics of retinal and the hydrogen-bonding properties of the retinal Schiff base and the internal water molecules. The change in case 1 and case 2 photoproduct yields between simulations with and without an explicit hydrogen-bond term indicates the importance of

this type of interaction in determining and stabilizing the isomerization results.

One step in this respect should base the simulation of retinal's photoisomerization on separate ground- and excited-state potential surfaces as outlined by Schulten et al. (1995) rather than employing a single surface, as in the present case. The simulations reported, here using a single potential energy surface, enforce a complete all-*trans*  $\rightarrow$  13-*cis* isomerization and, accordingly, favor case 1 photoproducts. Recent classical/quantum mechanical simulations on the three potential surfaces suggested in (Schulten et al., 1995) have indeed resulted in satisfactory quantum yields (in preparation).

As discussed in our previous study of the wild-type photoisomerization (Humphrey et al., 1995), the quantum yield of bR of  $0.64 \pm 0.04$  (Schneider et al., 1989; Govindjee et al., 1990; Tittor and Oesterhelt, 1990) indicates that many, but not all, of the photoreactions result in an isomerized retinal. The photoisomerization schedule employed here includes a step that introduces a bias toward completion of the all-*trans*  $\rightarrow$  13-*cis* reaction, and, in our simulations, the fraction of 13-*cis* isomers is close to or exceeds the observed quantum yield.

### Direction of photoisomerization

We have investigated the possibility that the direction of isomerization around retinal's C<sub>13</sub>-C<sub>14</sub> bond may determine bR's case 1 and case 2 photoproducts; a clockwise rotation (defined looking from the Schiff base nitrogen to the  $\beta$ -ionone ring of retinal) may favor one type of product, a counterclockwise rotation the other. For example, water W<sub>C</sub> may capture the Schiff base N-H<sup>+</sup> only during a clockwise isomerization, because in this case N-H<sup>+</sup> approaches W<sub>C</sub> closely, whereas it does not approach it in case of a counterclockwise all-*trans*  $\rightarrow$  13-*cis* isomerization. For this purpose we have monitored the rotational sense of all isomerizations occurring in our simulations, seeking a possible correlation of this property with the type of photoproduct formed. Very little correlation was found, as can be seen from the data in Table 1.

### Mechanism for reversed proton pumping

At pH 6.7, the D85N and D85T mutants of bR exist as a mixture of both all-*trans*, protonated retinal (bR<sub>trans</sub>) and all-*trans*, deprotonated retinal (M<sub>trans</sub>). Illuminating this mixture with blue light results in a proton current in the same direction as for wild-type bR (Tittor et al., 1994, 1995). In this case, blue light is absorbed by bR with deprotonated all-*trans* retinal, the latter absorbing near 410 nm; retinal photoisomerizes to the 13-*cis* isomer, becomes protonated from Asp-96, reverts thermally to all-*trans*, and forms again a mixture of protonated and deprotonated retinal. Illumination of the D85N and D85T mutants by yellow light excites the bR with protonated all-*trans*

retinal, but no steady proton current is generated. However, addition of blue light induces a proton current, albeit in a direction opposite the current of native bR (Tittor et al., 1994, 1995). In this case the protonated retinal photoisomerizes through absorption of yellow light, releases its proton toward Asp-96, absorbs in the deprotonated form a blue photon, and returns to the initial retinal all-*trans* isomer, forming again a mixture of protonated and deprotonated retinal. This surprising reversal of the proton pump direction of the D85N and D85T mutants of bR can be reconciled in a straightforward way with the appearance of case 1 photoproducts, as demonstrated in Fig. 5.

The model in Fig. 5 extends a suggestion by Tittor and co-workers (Tittor et al., 1994, 1995), in that it introduces the case 1 structure into a scheme given by these authors. We suggest that protonated all-*trans* retinal photoisomerizes to a case 1 product, as shown in Fig. 3 *b*. The case 1 geometry of retinal is well suited for deprotonation to Asp-96, as indicated in Fig. 5, leading to a deprotonated 13-*cis* retinal. In this protonation state the barrier for thermal isomerization around the C<sub>13</sub>-C<sub>14</sub> bond measures about 50 kcal/mol, i.e., for all practical purposes it is insurmountable. However, photoisomerization can occur when light in the 400 nm range (i.e., blue light) is provided. This leads back to unprotonated all-*trans* retinal, as shown in Fig. 5. The Schiff base nitrogen pointing toward the extracellular side can receive a proton from this direction, form the initial protonated all-*trans* retinal, and enter a new pump cycle, thus establishing a continuous inward current.

It is possible, however, to have case 2 photoproducts appear in this scheme, which would then simply return to the bR<sub>trans</sub> state because of the lack of a proton acceptor. However, case 2 photoproducts are much less likely to appear, because of the changed electrostatic environment of the retinal binding site, and the disruption of the water structure in this region. Conversely, it is possible for case 1 products to occur in a functional photocycle of native bR, and thermally reconvert back to the initial ground state while case 2 photoproducts continue the cycle. The quantum yield of the bR photocycle, which is less than unity ( $0.64 \pm 0.04$ ; Schneider et al., 1989; Govindjee et al., 1990; Tittor and Oesterhelt, 1990), suggests this as a possibility. Although the bR mutant simulations reported here do not model all of the steps in the suggested model of reverse proton pumping, they do provide a possible mechanism for the initiation of the observed reverse pumping in D85N and D85T mutants.

### Case 1 and case 2 photoproducts: both can have a functional role

The inverted pump cycle in Fig. 5 hinges on the formation of a case 1 photoproduct. The model is consistent with the suggestion that case 2 photoproducts in bR initiate an outwardly pumping photocycle and that mutations abolishing this photoproduct and favoring case 1 products lead to an

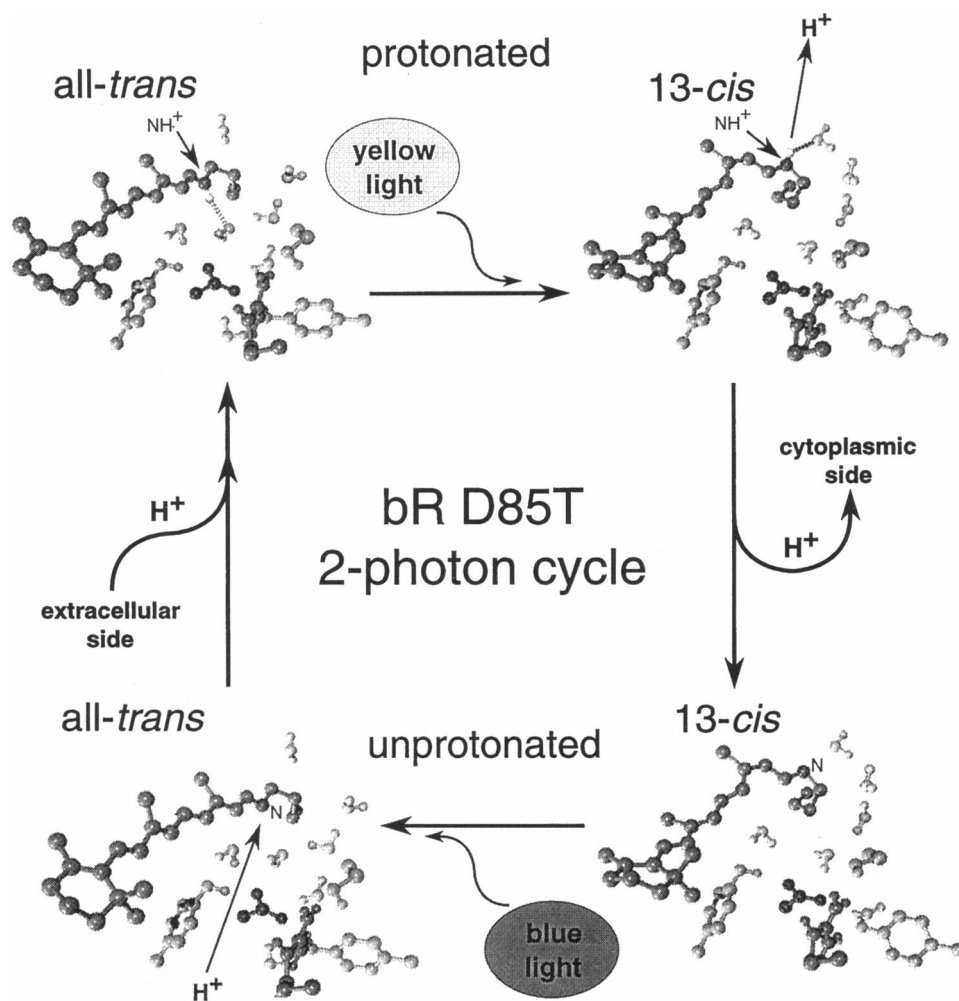


FIGURE 5 Suggested mechanism of reverse proton pumping of the bR D85T mutant. Protonated all-*trans* retinal (top left) absorbs yellow light and photoisomerizes to a case 1 product (top right). The N-H<sup>+</sup> bond points toward the cytoplasmic (top) direction and releases its proton to form the corresponding unprotonated retinal Schiff base (bottom right). The latter absorbs blue light and photoisomerizes to unprotonated all-*trans* retinal (bottom left), with the Schiff base nitrogen pointing toward the extracellular (bottom) direction; the chromophore is re-protonated, and the initial protonated all-*trans* chromophore (top left) is reformed.

inwardly pumping cycle under appropriate light conditions. The question arises why such control switching between two photoproducts and two very different cycles might be advantageous to the bacterial host.

Two answers suggest themselves. First, the protein halorhodopsin, a close analog of bR, lacks a negatively charged side group in place of Asp-85 in the retinal binding site. The protein shows the same reverse pump behavior as bR D85T mutants (Bamberg et al., 1992). Accordingly, the protein reverses the proton flow in the bacterial cell membrane under intense light conditions with both yellow and blue light present at sufficient intensities. Such reversal seems to be necessary to avoid overcharging the bacterial cell through a strictly unidirectional proton pump (Bamberg et al., 1992). One can conclude that the design of bR with two possible photoproducts, namely case 1 and case 2, lends itself to the design of halorhodopsin.

A second answer is also based on the fact that case 1 photoproducts either do not initiate proton pumping in the outward direction or, for some light conditions, initiate reversed proton pumping. The bistability of bR's photoproducts can induce a slippage in the proton pump (i.e., idle photocycles) by allowing a shift to case 1 products when a

sufficient membrane potential has been generated. This potential would, indeed, have the same effect as neutralizing the Asp-85 negative charge favoring formation of case 1 products. We conclude that the bistability reflected in the appearance of case 1 and case 2 photoproducts might be a desirable, if not necessary, inefficiency of biological proton pumps.

The authors wish to thank M. Sheves, T. Ebrey, S. Balashov, and R. Govindjee for numerous helpful discussions. All simulations reported here were carried out using Hewlett-Packard workstations operated by the Resource for Concurrent Biological Computing at the University of Illinois and Beckman Institute.

This work was supported by grants from the National Institutes of Health (PHS 5 P41 RR05969-04), the National Science Foundation (BIR-9318159), and the Roy J. Carver Charitable Trust.

## REFERENCES

- Balashov, S. P., R. Govindjee, E. S. Imasheva, S. Misra, T. G. Ebrey, Y. Feng, R. K. Crouch, and D. R. Menick. 1995. The two pK<sub>a</sub>'s of aspartate-85 and control of thermal isomerization and proton release in the arginine-82 to lysine mutant of bacteriorhodopsin. *Biochemistry*. 34:8820–8834.

- Bamberg, E., J. Tittor, and D. Oesterhelt. 1992. Light-driven proton or chloride pumping by halorhodopsin. *Proc. Natl. Acad. Sci. USA*. 90: 473–486.
- Brooks, B. R., R. E. Bruccoleri, B. D. Olafson, D. J. States, S. Swaminathan, and M. Karplus. 1983. CHARMM: a program for macromolecular energy, minimization, and dynamics calculations. *J. Comp. Chem.* 4:187–217.
- Brown, L. S., J. Sasaki, H. Kandori, A. Maeda, R. Needleman, and J. K. Lanyi. 1995. Glutamic acid 204 is the terminal proton release group at the extracellular surface of bacteriorhodopsin. *J. Biol. Chem.* 270: 27122–27126.
- Brünger, A. T. 1988. X-PLOR. The Howard Hughes Medical Institute and Department of Molecular Biophysics and Biochemistry, Yale University, New Haven, CT.
- Ebrey, T. 1993. Light energy transduction in bacteriorhodopsin. In *Thermodynamics of Membranes, Receptors and Channels*. M. Jacobson, editor. CRC Press, New York. 353–387.
- Govindjee, R., S. P. Balashov, and T. G. Ebrey. 1990. Quantum efficiency of the photochemical cycle of bacteriorhodopsin. *Biophys. J.* 58: 597–608.
- Govindjee, R., M. Kono, S. P. Balashov, E. Imasheva, M. Sheves, and T. G. Ebrey. 1995. Effects of substitution of tyrosine 57 with asparagine and phenylalanine on the properties of bacteriorhodopsin. *Biochemistry*. 34:4828–4838.
- Henderson, R., J. M. Baldwin, T. A. Ceska, F. Zemlin, E. Beckmann, and K. H. Downing. 1990. Model for the structure of bacteriorhodopsin based on high-resolution electron cryomicroscopy. *J. Mol. Biol.* 213: 899–929.
- Holz, M., L. A. Drachev, T. Mogi, H. Otto, A. D. Kaulen, M. P. Heyn, V. P. Skulachev, and H. G. Khorana. 1989. Replacement of aspartic acid-96 by asparagine in bacteriorhodopsin slows both the decay of the M intermediate and the associated proton movement. *Proc. Natl. Acad. Sci. USA*. 86:2167–2171.
- Humphrey, W., I. Logunov, K. Schulten, and M. Sheves. 1994. Molecular dynamics study of bacteriorhodopsin and artificial pigments. *Biochemistry*. 33:3668–3678.
- Humphrey, W., D. Xu, M. Sheves, and K. Schulten. 1995. Molecular dynamics study of the early intermediates in the bacteriorhodopsin photocycle. *J. Phys. Chem.* 99:14549–14560.
- Korenstein, R., and B. Hess. 1977. Hydration effects on *cis-trans* isomerization of bacteriorhodopsin. *FEBS Lett.* 82:7–11.
- Lanyi, J. K. 1992. Proton-transfer and energy coupling in the bacteriorhodopsin photocycle. *J. Bioenerg. Biomembr.* 24:169–179.
- Lozier, R. H., R. A. Bogomolni, and W. Stoeckenius. 1975. Bacteriorhodopsin: a light-driven proton pump in *Halobacterium halobium*. *Biophys. J.* 15:955–962.
- Maeda, A., J. Sasaki, Y. Yamazaki, R. Needleman, and J. K. Lanyi. 1994. Interaction of aspartate-85 with a water molecule and the protonated Schiff base in the L intermediate of bacteriorhodopsin—a Fourier-transform infrared spectroscopic study. *Biochemistry*. 33:1713–1717.
- Mogi, T., L. Stern, T. Marti, B. Chao, and H. Khorana. 1988. Aspartic acid substitutions affect proton translocation by bacteriorhodopsin. *Proc. Natl. Acad. Sci. USA*. 85:4148–4152.
- Needleman, R., M. Chang, B. Ni, G. Varo, J. Fornes, S. H. White, and J. K. Lanyi. 1991. Properties of Asp<sup>212</sup> → Asn bacteriorhodopsin suggest that Asp<sup>212</sup> and Asp<sup>85</sup> both participate in a counterion and proton complex near the Schiff base. *J. Biol. Chem.* 266:11478–11484.
- Nelson, M., W. Humphrey, A. Gursoy, A. Dalke, L. Kale, R. D. Skeel, and K. Schulten. 1996. NAMD—a parallel, object-oriented molecular dynamics program. *J. Supercomput. Appl.* 10:251–268.
- Oesterhelt, D., and W. Stoeckenius. 1973. Functions of a new photoreceptor membrane. *Proc. Natl. Acad. Sci. USA*. 70:2853–2857.
- Oesterhelt, D., J. Tittor, and E. Bamberg. 1992. A unifying concept for ion translocation in retinal proteins. *J. Bioenerg. Biomembr.* 24:181–191.
- Otto, H., T. Marti, M. Holz, T. Mogi, L. J. Stern, F. Engel, H. G. Khorana, and M. P. Heyn. 1990. Substitution of amino acids Asp-85, Asp-212, and Arg-82 in bacteriorhodopsin affects the proton release phase of the pump and the pK of the Schiff base. *Proc. Natl. Acad. Sci. USA*. 87:1018–1022.
- Papadopoulos, G., N. Dencher, G. Zaccai, and G. Büldt. 1990. Water molecules and exchangeable hydrogen ions at the active centre of bacteriorhodopsin localized by neutron diffraction. *J. Mol. Biol.* 214: 15–19.
- Richter, H.-T., L. S. Brown, R. Needleman, and J. K. Lanyi. 1996. A linkage of the pKa's of Asp-85 and Glu-204 forms part of the reprotonation switch of bacteriorhodopsin. *Biochemistry*. 35:4054–4062.
- Schneider, G., R. Diller, and M. Stockburger. 1989. Photochemical quantum yield of bacteriorhodopsin from resonance Raman scattering as a probe for photolysis. *Chem. Phys.* 131:17–29.
- Schulten, K., W. Humphrey, I. Logunov, M. Sheves, and D. Xu. 1995. Molecular dynamics studies of bacteriorhodopsin's photocycles. *Isr. J. Chem.* 35:447–464.
- Subramaniam, S., T. Marti, and H. G. Khorana. 1990. Protonation state of Asp (Glu)-85 regulates the purple-to-blue transition in bacteriorhodopsin mutants Arg-82 → Ala and Asp-85 → Glu: the blue form is inactive in proton translocation. *Proc. Natl. Acad. Sci. USA*. 87:1013–1017.
- Tittor, J., and D. Oesterhelt. 1990. The quantum yield of bacteriorhodopsin. *FEBS Lett.* 263:269–273.
- Tittor, J., D. Oesterhelt, and E. Bamberg. 1995. Bacteriorhodopsin mutants D85N, D85T, and D85,96N as proton pumps. *Biophys. Chem.* 56: 153–157.
- Tittor, J., U. Schweiger, D. Oesterhelt, and E. Bamberg. 1994. Inversion of proton translocation in bacteriorhodopsin mutants D85N, D85T, and D85,96N. *Biophys. J.* 67:1682–1690.
- Xu, D., C. Martin, and K. Schulten. 1996. Molecular dynamics study of early picosecond events in the bacteriorhodopsin photocycle: dielectric response, vibrational cooling and the J, K intermediates. *Biophys. J.* 70:453–460.
- Xu, D., M. Sheves, and K. Schulten. 1995. Molecular dynamics study of the M412 intermediate of bacteriorhodopsin. *Biophys. J.* 69:2745–2760.
- Zhou, F., A. Windemuth, and K. Schulten. 1993. Molecular dynamics study of the proton pump cycle of bacteriorhodopsin. *Biochemistry*. 32:2291–2306.